



ELSEVIER

Nuclear Instruments and Methods in Physics Research B 158 (1999) 31–38

**NIM B**  
Beam Interactions  
with Materials & Atoms

www.elsevier.nl/locate/nimb

# The ANSTO high energy heavy ion microprobe

Rainer Siegele <sup>\*</sup>, David D. Cohen, Nick Dytlewski

*Australian Nuclear Science and Technology Organisation, PMB 1, Menai 2234, NSW, Australia*

---

## Abstract

Recently the construction of the ANSTO High Energy Heavy Ion Microprobe (HIMP) at the 10 MV ANTARES tandem accelerator has been completed. The high energy heavy ion microprobe focuses not only light ions at energies of 2–3 MeV, but is also capable of focusing heavy ions at high energies with  $ME/q^2$  values up to 150 MeV amu and greater. First performance tests and results are reported here. © 1999 Elsevier Science B.V. All rights reserved.

---

## 1. Introduction

The Australian Nuclear Science and Technology Organisation (ANSTO) has a long tradition in low energy Ion Beam Analysis (IBA) and research on its 35 years old 3 MV Van de Graaff accelerator. In 1989 this IBA work was extended to higher energies and heavier ions with the installation of the 10 MV tandem accelerator ANTARES. This work includes both Elastic Recoil Detection Analysis (ERDA) [1] and Nuclear Reaction Analysis (NRA). However, with increased interest in analysing smaller structures in man made materials as well as geological, biological and archaeological samples, there is a growing demand for microanalysis. This demand has led to an increase in the number of proton microprobes around the world. ANSTO was among the first laboratories to use microscopic beams for IBA by

applying apertures to minimise the beam spot size rather than active focusing elements [2,3].

To continue this tradition, it was decided in late 1993 to add a high energy, heavy ion microprobe (HIMP) to the ANSTO IBA facilities [4]. The aim was not to duplicate existing proton microprobe facilities in Australia or internationally, but to design a microprobe that would utilise IBA techniques at high energies using heavy ions, which have become more common in the IBA community in recent years. In particular, these methods include high energy nuclear reactions and heavy ion ERDA to analyse a range of light elements such as H, C, N and O. The primary aim was to establish these heavy ion techniques on HIMP using moderate spot sizes between 5 and 20  $\mu\text{m}$ , with sufficient beam current to perform IBA in a reasonable time.

Reducing the beam spot size generally reduces the target current and thus the count rate in the detector. This of course increases the measurement time, but this can be overcome in different ways; (1) by a higher ion source brightness, (2) by larger solid angle detectors or (3) using IBA techniques

---

<sup>\*</sup> Corresponding author. Tel.: +61-2-9717-3967; fax: +61-2-9717-3257; e-mail: rns@ansto.gov.au

with higher reaction cross sections. Fig. 1 shows the reaction cross sections for various IBA techniques as a function of the atomic number of the target material. The cross-sections of most IBA-techniques increase proportionally to the square of the atomic number of the incident ion, thus making the use of heavy ions advantageous in microprobes. However, in order to assess the properties of a particular IBA technique under similar conditions, the cross sections for different projectiles should be compared at the same velocity. Fig. 1 shows the K and L X-ray production cross-sections for 3 MeV protons and 36 MeV carbon. There is a 10–100 fold increase in the X-ray production rate from protons to carbon, which gives ion induced X-ray emission analysis using heavy ions an advantage over proton PIXE. For comparison the figure also shows the cross sections for 2 MeV He RBS and 80 MeV Br ERDA. Again the figure shows a 10–100 fold increase in the cross section from 2 MeV RBS to ERDA using bromine. Because of the higher cross sections and the possibility to separate the signal resulting from different target atoms [1], heavy ion ERDA has certain advantages over RBS. Thus a heavy ion microprobe can make use of a higher cross section over the full range of elements by employing heavy ion ERDA and heavy ion PIXE, compared to RBS and proton PIXE.

The focusing quadrupoles for the High Energy Heavy Ion Microprobe were ordered from Oxford

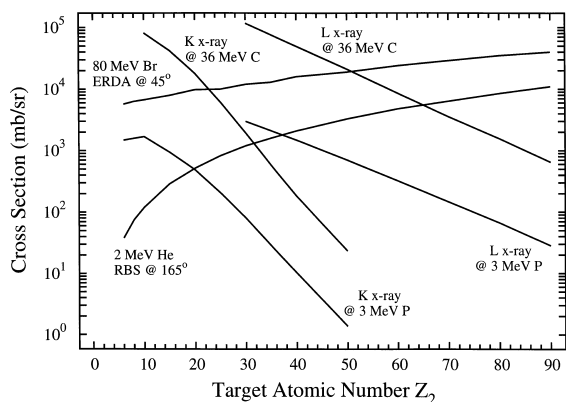


Fig. 1. Comparison of cross sections for various ion beam techniques using different ions.

Microbeams in 1996 and delivered in 1998. The microprobe was designed for a wide range of ions at various energies, with a maximum mass energy product  $ME/q^2 = 100$  MeV amu. This results in interesting new applications and allows for the application of a wide variety of ion beam analysis techniques in the microprobe field.

## 2. Description of the facility

The FN tandem accelerator from Rutgers University in USA was relocated to ANSTO in Australia in 1989 and has been operational since 1991. In 1996 the belt charging system was upgraded to a pelletron system, which produced improved terminal voltage stability of less than 1 kV at 8 MV. At the same time the installation of the high energy, heavy ion microprobe commenced. The tandem accelerator is equipped with two sputter ion sources and a charge exchange RF ion source. Most elements of the periodic table can be accelerated with reasonably high intensity.

The new high energy, heavy ion microprobe was located as close as possible to the high energy end of the accelerator to reduce the number of beam optical elements between the accelerator and the microprobe. The total length of the microprobe, from object slits to the centre of the target chamber is 7 m. The high energy ion beam coming from the accelerator is analysed and switched by a single 30° deflection magnet. The deflection is large enough to separate different charge states as well as neighbouring isotopes for most of the common ions used. Tests showed ion beam currents up to a few microamps are readily available at the entrance to the microprobe.

The major components of the high energy, heavy ion microprobe were supplied by Oxford Microbeams. Fig. 2 shows a schematic of the microprobe beamline. Both a Faraday cup and a beam profile monitor are located in front of the microprobe entrance. The ion beam enters the microprobe through a set of pre-slits, which limit the beam current impinging on the object slits. The pre-slits are adjustable 4-jaw apertures, which are also used to control the beam energy in slit control stabilisation mode. The pre-slits are immediately

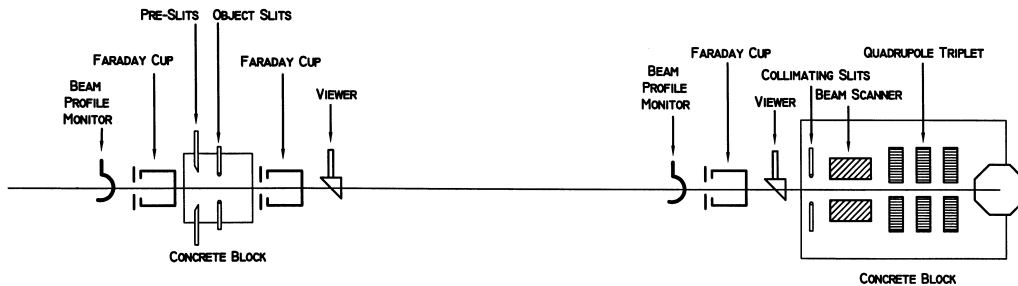


Fig. 2. Schematic of the microprobe beamline.

followed by the object slits. Both the object slits and the collimating apertures are 4-jaw rectangular beam defining apertures, consisting of highly polished stainless steel cylinders, in order to reduce the effects of surface roughness and scattering. To prevent vibrations the object slits are decoupled from the beamline by membrane bellows and mounted separately on a large solid concrete block.

A Faraday cup and a beam viewer are located after the object slits. These are used to optimise and align the beam passing through the object slits. Because of the long distance between object and collimating slits of 6.1 m, a second set of beam diagnostics, consisting of a beam profile monitor, a Faraday cup and a viewer are located in front of the collimating slits. These are used to fine tune the beam through the collimating slits.

The collimating apertures, beam scanning system, quadrupole triplet and the target chamber are all mounted on the same baseplate and mechanically isolated from the rest of the beamline by membrane bellows, as shown in Fig. 3. This whole end-station assembly is mounted on a concrete block, sitting on a layer of sand to prevent transmission of vibrations through the floor. The target chamber is pumped by a turbo-molecular pump, which is mounted on the floor and is mechanically isolated from the target chamber by a bellows system.

The collimating slits are immediately followed by the beam scanning system. A scanning system, designed to scan ion beams with a mass energy product of  $ME/q^2 = 100$  MeV amu over an area of  $1 \times 1$  mm<sup>2</sup> is under construction. The results presented in this paper, however, are obtained using a

scanning system, with a maximum scan area of only  $300 \times 300$   $\mu\text{m}^2$  for a mass energy product of less than 75 MeV amu.

The HIMP lens system consists of a magnetic quadrupole triplet from Oxford Microbeams (OM155). It uses the new heavy ion quadrupoles, which offer a higher focusing power, due a smaller pole gap of 8 mm. Oxford Microbeam guarantees a focussing power of the quadrupoles, that can focus ion beams with a  $ME/q^2 = 100$  MeV amu at a working distance of 150 mm. However, we were able to focus ion beams with a much larger  $ME/q^2 = 166$  MeV amu, without reaching the either saturation in the quadrupoles or the maximum current of the power supplies. The beam tube through the quadrupoles has an inner diameter of 4 mm, thus limiting the acceptance of the microprobe.

### 3. Target chamber assembly

The target chamber has a octagonal shape, with an inner diameter of 165 mm. Each face of the chamber is fitted with two 2 inch dependex ports, with one port at beamline height and one above this level, for electrical and mechanical feed-throughs. The target chamber is equipped with a surface barrier detector in a  $165^\circ$  backward geometry for heavy ion RBS. A peltier cooled pin-diode detector at a  $135^\circ$  back angle is used for heavy ion PIXE.

Fig. 3 also shows the microscope with a video camera used for ion beam focussing and target alignment. The chamber is equipped with an  $x$ - $y$ - $z$  manipulator for sample positioning. Above the

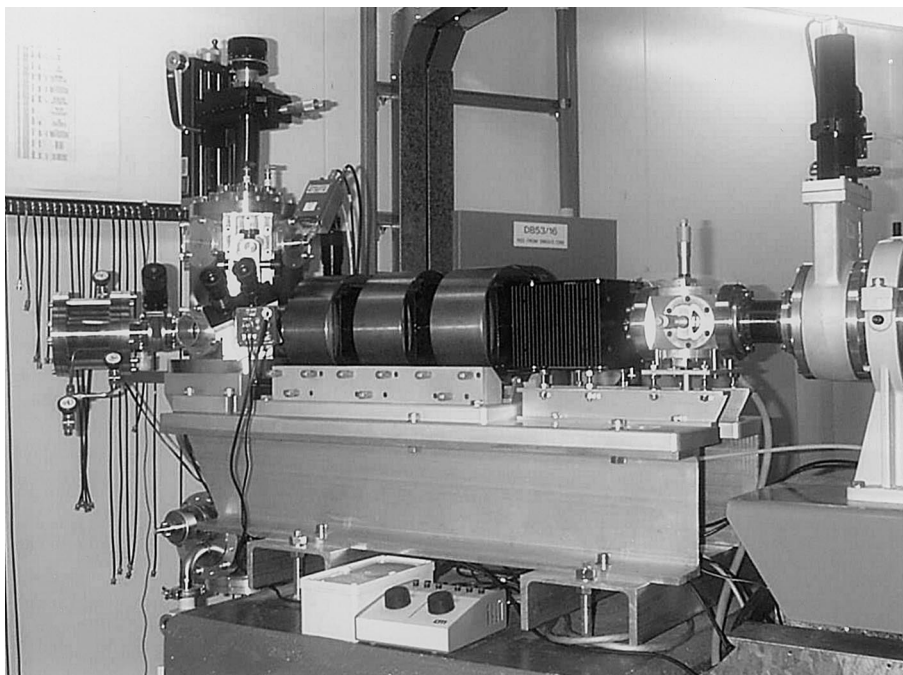


Fig. 3. The picture shows the microprobe endstation with the collimating slits, beam scanning system and the target chamber. In front of the target chamber the microscope is visible. The large chamber to the left of the target chamber is the  $dE-E$  ERDA detector.

target holder a small faraday cup is built into the shaft of the manipulator. This Faraday cup can be moved into the beam to allow accurate target current measurements.

The advantage of HIMP is the use of IBA techniques not accessible with proton microprobes, such as heavy ion ERDA. ERDA allows to separate the responses from various elements without the need to de-convolute overlaying energy signals [1]. A large solid angle  $dE-E$  detector for ERDA has recently been completed and will be tested in the near future. It is installed in a  $45^\circ$  forward geometry and is clearly visible to the left of the target chamber in Fig. 3. It is expected that

in the near future a STIM detector and a secondary electron detector will also be installed.

#### 4. Performance of the microprobe

Table 1 shows a list of ion beams with typical spot sizes that have been used with the microprobe to date. The performance of the microprobe has been tested by scanning a copper grid with various aperture acceptance settings. The beam size can be estimated from the profile across the edge of the copper grid. Tests were performed using acceptance settings for nominal spot sizes of 5, 10 and

Table 1  
List of ion beams so far focussed on the HIMP, with typical spot sizes achieved

Ion	Energy	$q$	$ME/q^2$	Spot sizes ( $\mu\text{m}$ )	Target current (nA)
I	64–80	7–9	125–166	15–30	1–10
Cl	37.5–45	4–5	63–82	7–30	1–25
C	20–35	3–4	26–27	7–30	1–25
He	8	2	8	15–25	0.5–5

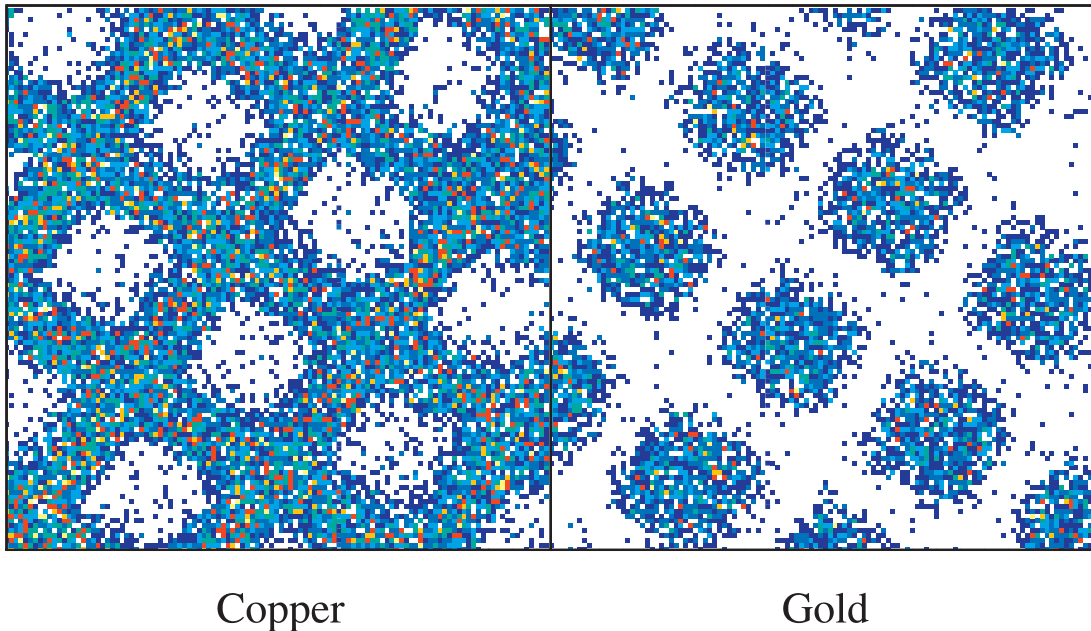


Fig. 4. Elemental maps of 200 lines/inch copper grid on a thin gold taken with 20 MeV C beam and a spot size of 17  $\mu\text{m}$ .

15  $\mu\text{m}$ , according to the manufacturers specifications, with 8 MeV He, 20–36 MeV C and 35 MeV Cl beams. Fig. 4 shows a typical surface images of a 200 lines/inch copper grid on silicon with 127  $\mu\text{m}$  spacing and 40  $\mu\text{m}$  diameter wire. The copper grid was placed on a silicon wafer with a thin gold surface layer. The images show results using RBS with 20 MeV C over a total scan area of  $400 \times 400 \mu\text{m}^2$ . A line scan under the same conditions is shown in Fig. 5. The analysis of the line scan yields a spot size of 17  $\mu\text{m}$ , which is very close to the expected spot size value of 15  $\mu\text{m}$ , calculated from the acceptance parameters. Spot size measurements with acceptance settings for 5  $\mu\text{m}$  spot sizes yielded measured spot sizes of around 7  $\mu\text{m}$ . This demonstrates that spot sizes down to 7  $\mu\text{m}$  are available with sufficient beam current to perform RBS experiments.

## 5. Results

In a first measurement the diffusion of strontium in cement pastes was investigated. The pictures in Fig. 6 show calcium, silicon, iron and

strontium images in cement pastes with zeolite inclusions. The left side of each of the figures represents the surface of the sample, that was exposed to a  $\text{SrCl}_2$  solution. The maps show a  $300 \times 300 \mu\text{m}$  area. Overlaid onto the images are the line profiles for each of those elements.

The calcium profile in Fig. 6a shows an increase in the Ca concentration away from the surface, but also strong variations across the sample. The lower

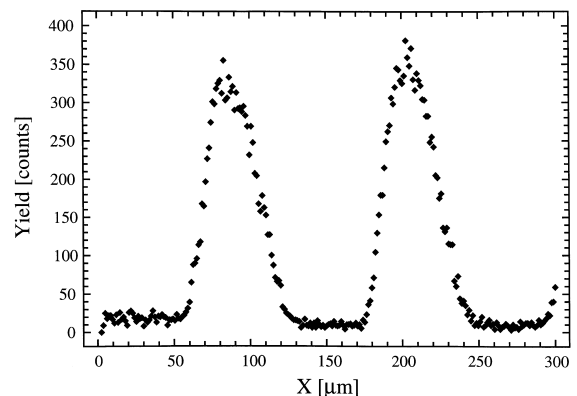


Fig. 5. Line scan on the sample shown in Fig. 4 taken under the same conditions.

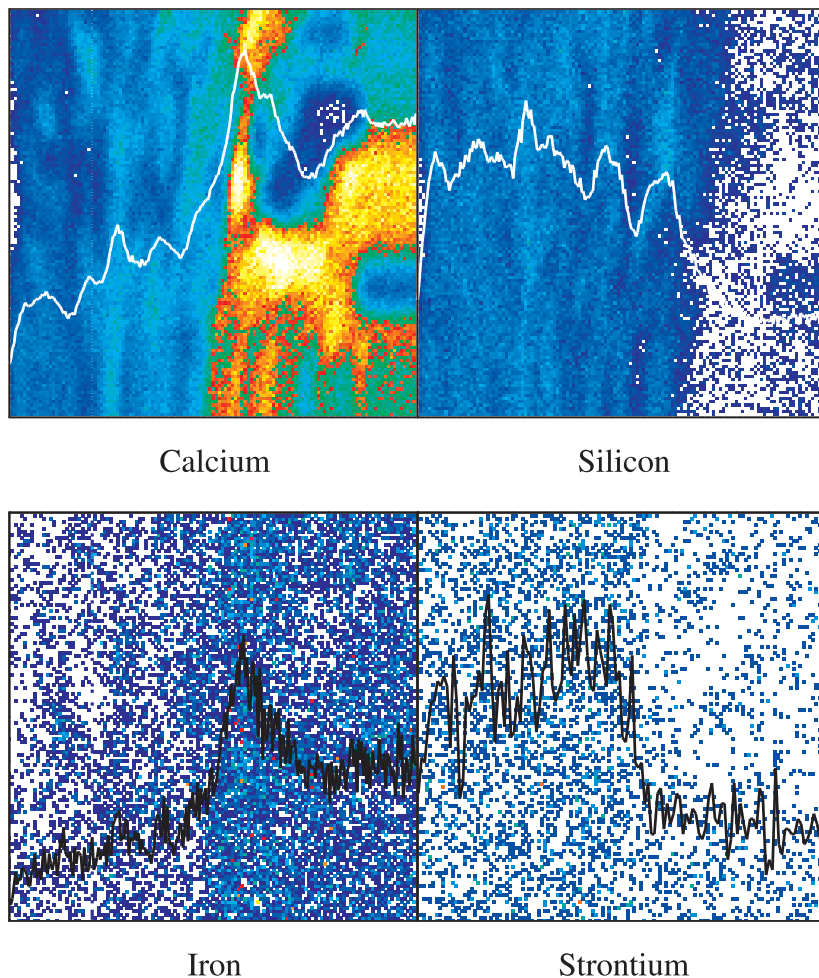


Fig. 6. Elemental maps of a cement paste sample, after exposure to a  $\text{SrCl}_2$  solution. The elemental maps are overlaid with the profiles along the  $x$ -axis.

Ca content near the surface is caused by the leaching of Ca, while the variations across the sample are due to the grainy structure and zeolite inclusions. The silicon concentration (Fig. 6b), however, is larger at the surface, which is due to the loss of Ca, since Si and Ca are the major constituents of the cement pastes. The iron (Fig. 6c) content shows a similar behaviour as Ca, indicating that Fe is also leached together with the Ca. The strontium profile (Fig. 6d) shows the area over which the Sr has diffused into the sample, during exposure to the  $\text{SrCl}_2$  solution.

In another experiment mineral grains of Ilmenite ( $\text{FeTiO}_3$ ) were investigated. Fig. 7 shows titanium and iron surface distribution images of a mineral grain with a diameter of roughly  $300 \mu\text{m}$ . The figure shows an area in the upper right, with no titanium and much lower iron concentration compared to the rest of the grain. A similar area is also visible in the centre left. Both areas show up as transparent inclusions in an optical microscope. They are silicate inclusions in the grain, which do not show in the elemental maps, since the data were taken with a  $250 \mu\text{m}$  Kapton filter in front of

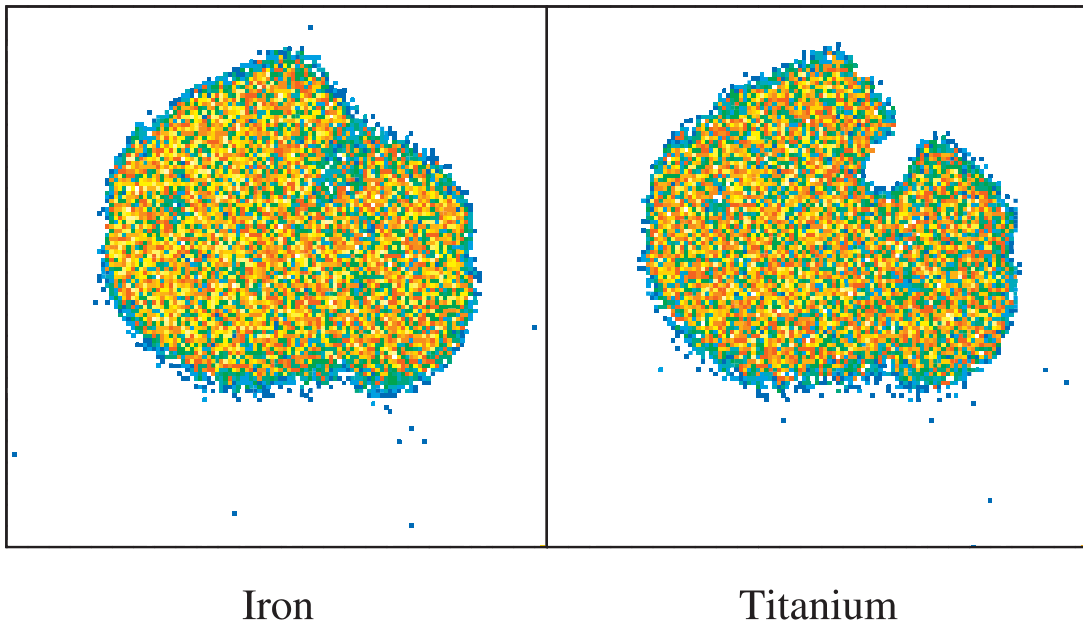


Fig. 7. Titanium and iron maps of a mineral sand grain, taken with a 36 MeV C and a spot size of 15  $\mu\text{m}$ .

the X-ray detector, absorbing most of the low energy Si X-rays.

The last example shows a high energy ( $\alpha,\alpha$ ) resonance scattering spectrum of tantalum covered with a thin layer of  $\text{Ta}_2\text{O}_5$ . The spectrum of Fig. 8 was taken using a 7.6 MeV He beam. At this energy a ( $\alpha,\alpha$ ) resonance results in 100 times in-

creased (above Rutherford) cross section for oxygen [5]. The peak in the spectrum is due to oxygen in the  $\text{Ta}_2\text{O}_5$ . This strong resonance was used to confirm the homogeneity of the oxide layer by scanning the beam over the entire sample area (5 mm diameter).

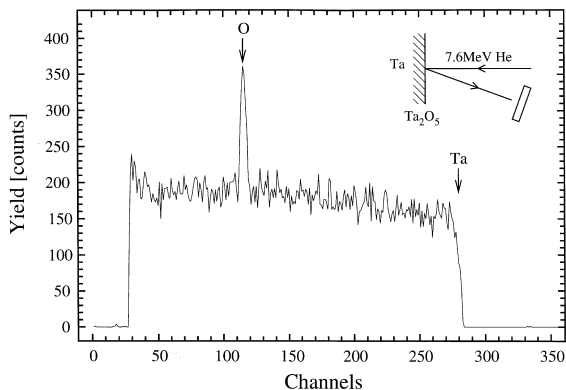


Fig. 8. RBS spectrum of a Ta sample covered with a thin  $\text{Ta}_2\text{O}_5$  layer. The spectrum was taken with a 7.6 MeV He beam showing the enhanced yield for oxygen caused by a strong resonance at this energy.

## 6. Conclusions

We have designed and built a new high energy, heavy ion microprobe beamline on the 10 MV ANTARES Tandem accelerator at ANSTO. The construction of the beamline has been completed and the microprobe is at the moment undergoing intensive testing with various ions and energies. Tests have shown that the maximum mass energy product that can be focused is well in excess of the specification of 100 MeV amu. So far a wide range of spot sizes, from 5–30  $\mu\text{m}$  in diameter, have been achieved. The microprobe has been extensively tested using He, C, Cl, Br and I ions at energies ranging from 8–80 MeV. Spot sizes as small as 7  $\mu\text{m}$  have been obtained with sufficient current to perform IBA analysis. So far high energy heavy

ion backscattering and PIXE detection systems are operational, with STIM and ERDA detection systems close to completion.

### **Acknowledgements**

We want to thank G. Legge at the Melbourne Microprobe group, as well as A. Dymnikov for many valuable discussions about the design of ion microprobes. The authors would also like to thank Hans Noorman, David Garton and Alex Craol for their help in constructing the beamline and the Tandem Accelerator Operations Team for their efforts. We also want to thank G. Grime and

M. Dawson for their support during construction and commissioning phases of the microprobe.

### **References**

- [1] J.W. Martin, D.D. Cohen, N. Dytlewski, D.B. Garton, H.J. Withlow, G.J. Russel, *Nucl. Instr. and Meth. B* 94 (1994) 277.
- [2] B.K. Mak, J.R. Bird, T.M. Sabine, *Nature* 211 (1966) 738.
- [3] P.B. Price, J.R. Bird, *Nucl. Instr. and Meth.* 69 (1969) 277.
- [4] G.J.F. Legge, A. Dymnikov, G. Moloney, A. Saint, D.D. Cohen. *Proceedings Ninth Australian Conference on Nuclear Techniques of Analysis*, 1995, p. 65.
- [5] F.J.D. Almeida, J.A. Davies, T.E. Jackman, *Nucl. Instr. and Meth. B* 82 (1993) 393.